SIN-CHN SCIENTIFIC PRESS PTE.LTD.

Molecular & Cellular Biomechanics 2024, 21(3), 591.
https://doi.org/10.62617/mcb591

Article

Establishment of a decision tree prediction model for the treatment of intracranial aneurysms using temperature-sensitive embolic agents based on geometric features

Miao Liu[1], Bingli Yu[1], Yakun Wang[2,*]

[1] Academy of Medical Engineering and Translational Medicine, Tianjin University, Tianjin 300072, China
[2] Cardiovascular Center, Tianjin Children's Hospital, Tianjin 300074, China
*** Corresponding author:** Wang Yakun, 2021235020@tju.edu.cn

CITATION

Liu M, Yu B, Wang Y. Establishment of a decision tree prediction model for the treatment of intracranial aneurysms using temperature-sensitive embolic agents based on geometric features. Molecular & Cellular Biomechanics. 2024; 21(3): 591. https://doi.org/10.62617/mcb591

ARTICLE INFO

Received: 22 October 2024
Accepted: 28 October 2024
Available online: 5 December 2024

Abstract: Intracranial aneurysms are abnormal expansions caused by weak arterial walls, which can lead to subarachnoid hemorrhage and high mortality rates in severe cases. Its clinical treatment commonly involves transcatheter arterial embolization. Compared with mainstream coil materials, the use of emerging temperature-sensitive embolic agents has higher occlusion rates, and reduces stress on the aneurysm wall, with lower toxicity and better treatment outcomes. However, due to the irreversibility of the coagulation process, there is a risk of unintended embolization of distal branches, limiting their clinical applicability. In order to obtain the applicable conditions of the temperature-sensitive embolic agent and further improve its applicability, this study employed the Euler two-phase flow model to simulate the embolization process of these agents. Based on the simulation results and geometric features of the cases, a decision tree model was established. Cross-validation revealed an overall success rate of 78.57% for predicting treatment applicability, with a sensitivity of 71.4%, specificity of 81.0%, and an F1 score of 62.5%. This decision tree model can serve as an auxiliary tool in the clinical treatment of intracranial aneurysms, allowing for the selection of cases suitable for temperature-sensitive embolization based on patients' specific geometric features obtained from imaging, thereby enhancing the success rate of surgical procedures.

Keywords: intracranial aneurysm; temperature-sensitive embolic agents; Euler two-phase flow; decision tree model; geometric features

1. Introduction

Intracranial Aneurysm (IA) is an abnormal dilatation caused by a weakness in the arterial wall, with sizes ranging from less than 0.5 mm to more than 25 mm [1]. Clinically, IAs are mainly classified into four types based on their geometric morphology: saccular aneurysms, microaneurysms, giant intracranial aneurysms, and fusiform intracranial aneurysms [2]. Currently, clinical treatment methods for IA can be broadly categorized into minimally invasive endovascular embolization and open surgical clipping. The goal of both methods is to remove the aneurysm from the blood circulation and prevent its rupture while providing a durable therapeutic effect [3]. Notably, open surgery is invasive and carries a higher risk of complications. In contrast, endovascular treatment is less traumatic, significantly reducing the treatment mortality rate and offering better clinical outcomes [4,5].

Currently, the challenges of IA treatment are focused on reducing recurrence rates and complications. These challenges not only affect the recovery and prognosis of patients, but also bring significant difficulties in clinical treatment [6]. In the history

of endovascular treatment of IA, with the continuous development of minimally invasive interventional techniques, a variety of endovascular therapeutic techniques, such as flow diversion and intracapsular flow disrupters, have gradually emerged [7,8]. However, these technologies have their limitations. For example, flow diversion may encounter severe tortuosity during deployment, leading to suboptimal results, and require patients to undergo prolonged dual antiplatelet therapy, which increases the risk of bleeding. Meanwhile, intracapsular flow disrupters are limited by aneurysm-specificity, which affects their generalizability [6]. In terms of embolic materials, a variety of materials for transcatheter arterial embolization have emerged, such as metal coils, injectable embolic agents, hydrogels, and new-generation embolic agents [3]. Although metal coils are a commonly used treatment, they are associated with a number of known complications such as bleeding, spring coil displacement, compaction, and recanalization. In contrast, liquid embolic agents (e.g., Onyx) have demonstrated better occlusion in filling the aneurysm lumen and are able to reduce the risk of rupture by reducing the stress on the aneurysm wall [9–11]. In response to these limitations of existing methods, temperature-sensitive embolic agents have been proposed as a new therapeutic option. Not only do temperature-sensitive embolic agents offer the advantages of liquid embolic agents, their good biocompatibility and low toxicity give them the potential to further minimize complications. As more and more temperature-sensitive embolic agents are developed and progressively attempted to be applied in embolization therapy for IA, they may provide new ideas and directions to address current therapeutic challenges [12–14].

However, temperature-sensitive embolic agents also face various technical limitations in practical applications, and thus have not been widely used in the embolization treatment of IA, such as the irreversibility of the embolic agent during the solidification process. Specifically, once the solidified polymer is delivered into the aneurysm, it cannot be repositioned or retrieved [11]. The risk of potential embolism of distal branches is similar to that of liquid embolic agents. Murayama et al. found in several studies that the rate of embolic material migrating to the parent vessel when using the Onyx liquid embolization system ranged from 9% to 33%, which could lead to occlusion of the parent vessel and trigger ischemic stroke [15]. Furthermore, blood flow within intracranial aneurysms is complex, making it highly likely for embolization failures to occur during the surgical process. Numerous hemodynamic studies have shown that Computational Fluid Dynamics (CFD) simulations are helpful in understanding the detailed blood flow characteristics of intracranial aneurysms [16–21]. These simulations can accurately describe the hemodynamics and arterial wall mechanical behavior, helping physicians in understanding the changes in the aneurysm under different blood flow and pressure conditions [22]. Successful simulations can predict the future expansion trends and potential rupture risks of the aneurysm, providing a basis for optimizing surgical and interventional treatment plans [23–25]. Therefore, conducting CFD simulations preoperatively to obtain virtual treatment outcomes for embolization therapy is necessary.

In the CFD computational methods, the Eulerian two-phase flow model has been validated by multiple studies in simulating the diffusion phenomena of embolic agents in blood, demonstrating its reliability and rationality. Ostrowski et al. analyzed a

numerical computational fluid dynamics model of pulsatile blood flow, indicating that this model can accurately simulate the injection and distribution of embolic agents in cerebral vessels [26]. Orlowski et al. used the Eulerian method to simulate the changes in blood flow in cerebral vessels after the obstruction of arteriovenous malformations and the delivery of embolic liquids [27]. Zhang et al. utilized the Eulerian model to simulate the diffusion behavior of liquid embolic agents during the treatment of cerebral arteriovenous malformations [28]. The Eulerian two-phase flow model shows promising application prospects and a solid scientific basis for simulating treatment in intracranial aneurysms. This paper uses the CFD results from the Eulerian two-phase flow as the basis for assessing treatment applicability, reasonably categorizing the treatment outcomes.

CFD holds significant importance in predicting treatment outcomes; however, it often faces high time and computational costs, limiting its direct application in clinical settings. Therefore, it is particularly important to construct more efficient predictive models. When using temperature-sensitive embolic agents to treat IA, the embolic agent is in a liquid state during the initial injection, coupling with the surrounding blood and significantly affecting the blood flow patterns. Furthermore, there is rich evidence that the vascular geometry has a substantial impact on the hemodynamics of intracranial aneurysms. The complexity and variability of vascular geometry directly influence the distribution and velocity of blood flow, while different geometric structures determine distinct flow patterns, which can affect the distribution of the embolic agent and, consequently, the therapeutic efficacy [29–31]. Thus, it is reasonable to rely solely on these geometric features to predict treatment effectiveness. Based on this, this paper establishes a decision tree model based on geometric features, using simulation results as the basis for assessment, aiming to quickly determine the treatment applicability through the geometric parameters of cases to provide effective support for clinical decision-making. The decision tree method is a commonly used data mining technique for building classification systems based on multiple variables or developing predictive algorithms for target variables [32]. This paper employs the decision tree model as the final binary classification model, where the geometric and computational parameters of the aneurysm and parent artery serve as input variables, based solely on geometric structure, with CFD results used as the basis for determining positive and negative examples.

2. Materials and methods

This study conducted virtual treatments for 28 patients with specific intracranial aneurysms (three computational models were carried out for each case according to different boundary conditions, i.e., 84 computational models were carried out) and analyzed the simulation results. The aim was to explore the factors influencing the success of embolization treatment using temperature-sensitive embolic agents for intracranial aneurysms. Based on the simulation results, a rapid reconstruction and screening tool identified by geometric information was established. This study can be summarized as a binary classification problem influenced by multiple factors regarding the success of the embolization treatment.

2.1. Data sources

The CADA dataset (https://cada-rre.grand-challenge.org/) was acquired using the digital subtraction AXIOM Artis C-arm system, with a rotation acquisition time of 5 seconds, resulting in a total of 126 frames (each frame capturing 190° or 1.5°, 1024 × 1024 pixel matrix, 126 frames). Post-processing was performed using LEONARDO InSpace 3D (Siemens, Forchheim, Germany). Contrast agent (Imeron 300, Bracco Imaging Deutschland GmbH, Germany) was manually injected into the internal carotid artery (for anterior aneurysms) or vertebral artery (for posterior aneurysms). A volume reconstruction was performed on the regions of interest selected by neurosurgeons, generating a three-dimensional stack of 440 image slices, with an in-plane matrix of 512 × 512 voxels and a voxel size of 0.25 mm [33].

2.2. Virtual treatment method based on Eulerian two-phase flow

2.2.1. Basic assumptions

(1) This study ignores the deformation of aneurysm and microcatheter caused by pressure, assumes that the vessel wall and microcatheter are rigid structures, and focuses mainly on the coupling of blood and embolic agent.

(2) The coagulation of temperature-sensitive embolic agents is mainly affected by temperature, and in this study, it is assumed that the temperature at which the embolic agent coagulates is reached after 60 s. Therefore, during the process of bolus injection (i.e., the first 60s), the temperature-sensitive embolic agent is in the liquid phase.

(3) It is assumed that the kinematic viscosity coefficient of blood remains constant during bolus agent injection. In the previous assumption, it was mentioned that the present study ignored the effect of energy, so the present study's research considered the blood viscosity and the viscosity of the temperature-sensitive bolus agent to be constant in the first 60 s. Therefore, this study set the bolus agent to fill the entire aneurysm in 60 s, and the injection rate is shown in equation (1):

$$V_{inject} = \frac{V_{anu}}{\pi r_{pipe}^2 \times 60} \tag{1}$$

where, V_{anu} is the volume of the aneurysm and r_{pipe} is the radius of the microcatheter for injection (as shown in **Figure 1a**), which was taken as 0.43 mm in this study.

(4) In this study, it is assumed that the vessel wall and microcatheter surface are no-slip boundary conditions.

2.2.2. Computational model design

(1) Use incompressible Newtonian fluid to represent blood

Blood viscosity models can be categorized into two main groups, namely Newtonian and non-Newtonian viscosity models. The use of multiphase non-Newtonian pulsating fluids to represent blood flow mainly assumes that blood consists of red blood cells and white blood cells, which are therefore elastic cells suspended in a Newtonian fluid called plasma (continuous phase). Due to the multiphase nature of blood, it is clear that blood viscosity will be controlled by the behavior of its microstructural components.

Most numerical simulations of intracranial aneurysms assume blood as a Newtonian fluid when solving the Navier-Stokes equations. The focus of this study is mainly on the coupling of blood and embolic agent, and Newtonian fluid can fulfill the needs of this study, so an incompressible Newtonian fluid is used to represent blood in this study.

(2) Use of laminar flow model

The focus of this study is to simulate the injection process of embolic agents in intracranial aneurysms. In order to simplify the calculations and efficiently simulate the interaction between blood and embolic agents, a laminar flow model was chosen for this study.

Within an intracranial aneurysm, blood flow usually presents as low Reynolds number flow. The computational results showed that the Reynolds numbers of the regions inside and around the aneurysm were lower than 2000, indicating that the flow in these regions was mainly in the laminar flow state. Therefore, the laminar flow model can effectively describe the flow characteristics of blood flow.

(3) Use of transient model

In this study, a transient model was used to accurately simulate the dynamic behavior of temperature-sensitive embolic agents in intracranial arteries. The transient model was able to capture the time-dependent characteristics of the bolus agent during injection and diffusion, and the total computation time was 60 s from the time the bolus agent was pushed out of the microcatheter.

(4) Relevant parameter settings

According to the assumptions in section 2.2.1, the research in this study set the blood density to 1060 kg/m^3; the blood kinematic viscosity to 0.0035 (Pa·s); and the viscosity of the embolic agent to 0.015 (Pa·s) [28].

2.2.3. Computational model solution

This study uses the Eulerian two-phase flow model for fluid dynamics simulations to simulate the embolization treatment process, employing the three-dimensional Navier-Stokes (NS) equations to model the fluid phase. The solid phase is simulated by solving the momentum equation and the continuity equation. Numerical solutions are performed using the simulation software FLUENT [34].

For the fluid phase, the continuity equation and momentum equation are represented by Equations (2) and (3), respectively.

$$\frac{\partial\left(\alpha_f \rho_f\right)}{\partial \mathrm{t}} + \nabla \cdot \left(\alpha_f \rho_{f u_f}\right) = 0 \tag{2}$$

$$\frac{\partial\left(\alpha_f \rho_f u_f\right)}{\partial t} + \nabla \cdot \left(\alpha_f \rho_f u_f \otimes u_f\right) = -\alpha_f \nabla P + \mu_f \nabla^2 u_f + F_{f,int} \tag{3}$$

For the solid phase, the continuity equation and momentum equation are represented by Equations (4) and (5), respectively.

$$\frac{\partial(\alpha_s \rho_s)}{\partial t} + \nabla \cdot (\alpha_s \rho_s u_s) = 0 \tag{4}$$

$$\frac{\partial(\alpha_s \rho_s u_s)}{\partial t} + \nabla \cdot (\alpha_s \rho_s u_s \otimes u_s) = -\alpha_s \nabla P + F_{s,int} \quad (5)$$

Where α_f and α_s represent the volume fractions of the fluid phase and solid phase, respectively; ρ_f and ρ_s are the corresponding densities; u_f and u_s denote the velocity fields of each phase; P is the shared pressure field; μ_f represents the dynamic viscosity of the fluid phase; and $F_{f,int}$ and $F_{s,int}$ are the interaction forces between the fluid phase and solid phase, respectively.

2.3. Geometric parameters and boundary conditions

After analysis, the main factors influencing the success of liquid embolic agent embolization are the geometric parameters and boundary conditions.

This study selects the following geometric parameters to explore the impact of geometric factors on the success of embolization treatment: the volume of the aneurysm (V_{anu}), aneurysm centerline length ($anu_{l_{centerline}}$), the maximum cross-sectional radius of the aneurysm (anu_r^{max}), the mean cross-sectional radius of the aneurysm (anu_r^{mean}), and the mean cross-sectional radius of the parent artery ($vessel_r^{mean}$) to represent their absolute values. Additionally, the study uses the ratio of the mean cross-sectional diameter of the aneurysm to the centerline length ($ratio_{anu_r^{mean}}^{anu_{l_{centerline}}}$), the cosine of the angle between the centerline of the parent vessel and the aneurysm centerline (cos_{vessel}^{anu}), and the ratio of the mean radius of the aneurysm to the mean radius of the parent artery ($V_r atio_{vessel}^{anu}$) to represent relative positions and relative sizes. The geometric parameters of the aneurysm are shown in **Figure 1**.

$ratio_{anu_r^{mean}}^{anu_{l_{centerline}}}$ characterizes the morphology of the aneurysm, as is shown in Equation (6). The smaller the value, the more "elongated" the aneurysm becomes.

$$ratio_{anu_r^{mean}}^{anu_{l_{centerline}}} = \frac{2 \times anu_r^{mean}}{anu_{l_{centerline}}} \quad (6)$$

$V_r atio_{vessel}^{anu}$, as is shown in Equation (7), indicates that the larger the value, the greater the size of the aneurysm relative to the parent artery.

$$V_{ratio_{vessel}}^{anu} = \frac{anu_{l_{centerline}} \times anu_r^{mean}}{(vessel_r^{mean})^2} \quad (7)$$

Related studies indicate that the relative position and size of the parent artery and the aneurysm determine their hemodynamic patterns [34]. Therefore, this study performs a dimensional analysis of the geometric parameters of the aneurysm and the parent artery to further explore the impact of their relative position and size on the outcomes.

The boundary conditions include the injection velocity and the insertion position of the microcatheter during injection. In this study, all outlet boundary conditions are the same, with a reference pressure of 0 at the outlet. Therefore, for the same case, the only influencing factor that varies is the insertion position of the microcatheter. Three insertion positions of the microcatheter are selected for calculations: the base of the

neck of the aneurysm, the middle of the aneurysm cavity, and deep within the aneurysm.

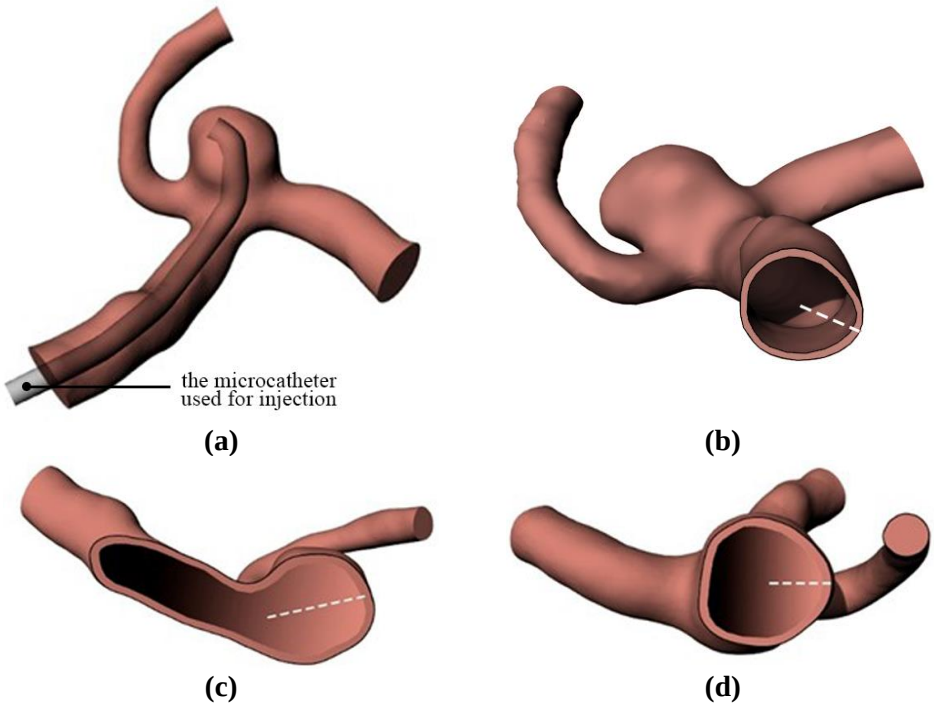

Figure 1. Schematic diagram of aneurysm geometric parameters. **(a)** Overall morphology of the microcatheter and aneurysm; **(b)** dashed line indicates the radius of the parent artery; **(c)** dashed line indicates the centerline of the aneurysm; **(d)** dashed line indicates the radius of the aneurysm.

2.4. Establishment of the decision tree model

2.4.1. Discretization of parameters

In constructing the predictive decision tree model for the treatment of intracranial aneurysms using temperature-sensitive embolic agents, this study employs K-means clustering for the discretization of cases to enhance the model's predictive accuracy and interpretability. The K-means clustering algorithm is a widely used unsupervised learning method aimed at grouping case data into K clusters, thereby aggregating cases with similar characteristics. To determine the optimal number of clusters, this study utilizes the silhouette coefficient method. The silhouette coefficient is an important metric for evaluating clustering quality, measuring the similarity of cases within a cluster compared to cases in other clusters by combining the cohesion within the cluster and the separation from other clusters. Its value ranges from [−1, 1].

Specifically, the cohesion a represents the average distance between a case and other cases within its cluster, as shown in Equation (8):

$$a(i) = \frac{1}{|C_i| - 1} \sum_{j \in C_i, i \neq j} d(i,j) \tag{8}$$

Where C_i is the cluster that contains case i, $|C_i|$ is the number of cases in cluster C_i, and $d(i,j)$ is the distance between cases i and j $(i \neq j)$ to ensure that case i is not included in the calculation of the average distance.

The separation b refers to the average distance between a case and the nearest cases from other clusters. It is calculated by determining the average distance of the case to all cases in other clusters and taking the minimum value as b, as shown in Equation (9):

$$b(i) = \min_{k \neq i} \left(\frac{1}{|C_k|} \sum_{j \in C_k} d(i,j) \right) \tag{9}$$

The calculation of the silhouette coefficient is shown in Equation (10). The value of the silhouette coefficient will assist in selecting the optimal K value, thereby ensuring that the model can more accurately reflect the impact of different geometric features on the treatment outcomes when predicting the suitability of temperature-sensitive embolic agents.

$$s = \frac{b - a}{\max(a, b)} \tag{10}$$

For each parameter, this study calculated the number of clusters ranging from [2, 6] and sorted the clusters in ascending order based on the size of the dimensionless parameters. Among them, a higher cluster index indicates a larger value of the dimensionless parameter. The discretization information for each parameter is shown in **Figure 2**.

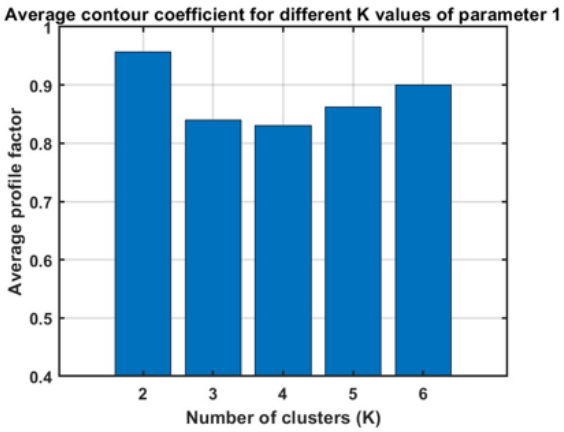

(a)

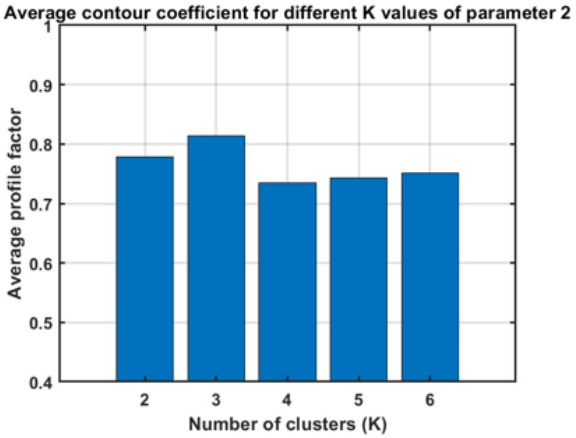

(b)

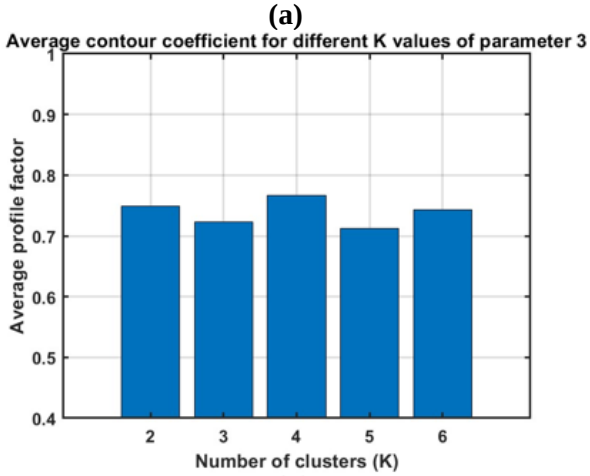

(c)

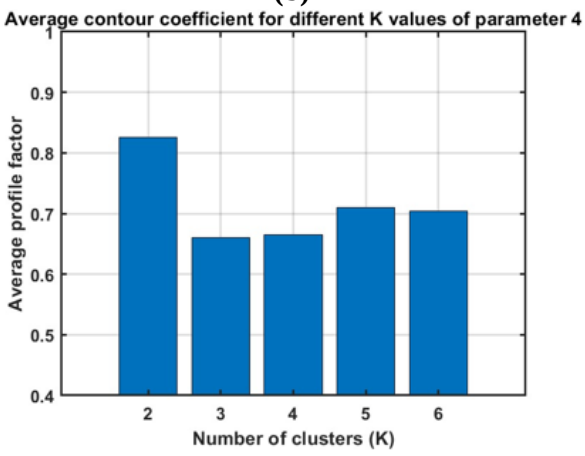

(d)

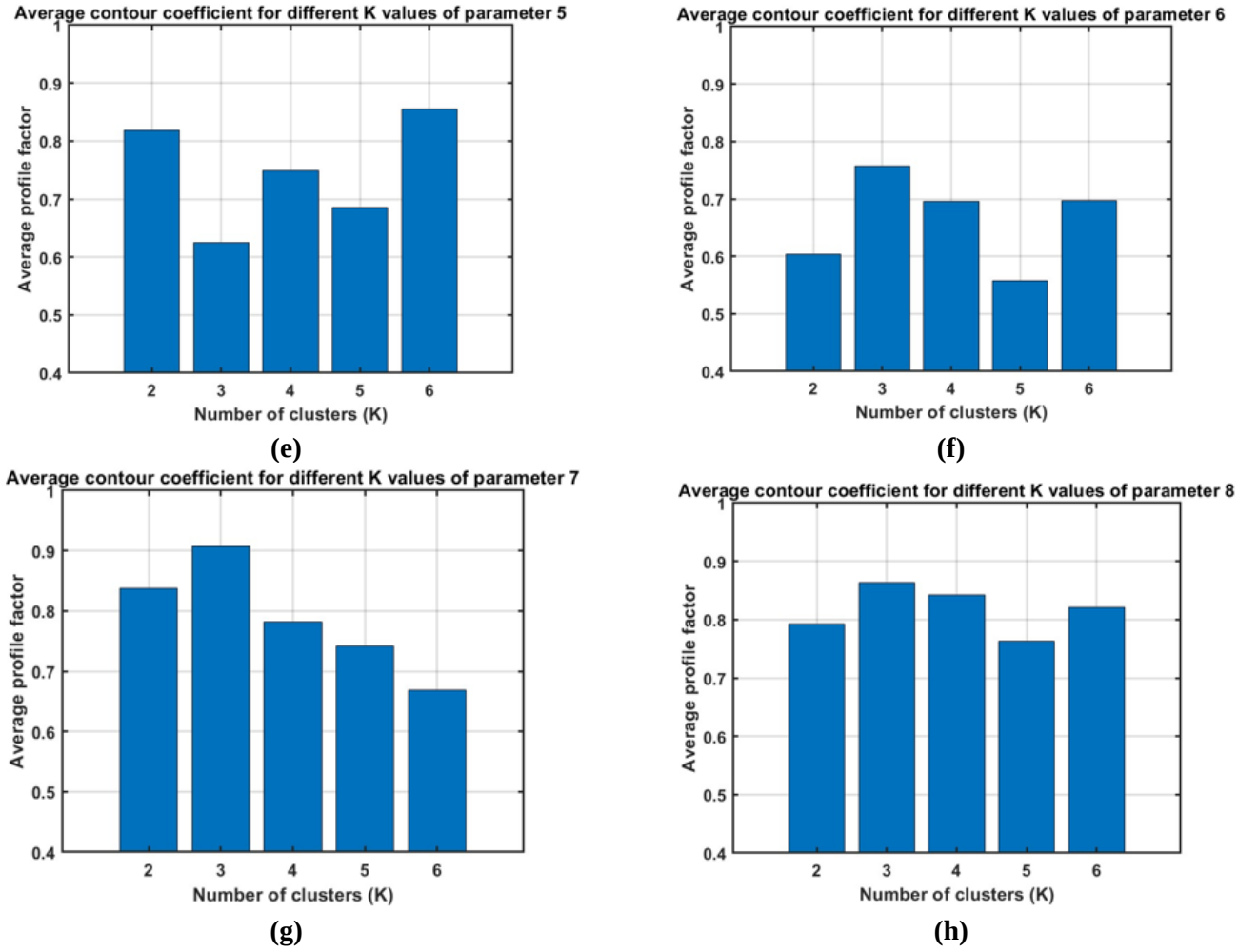

Figure 2. Discretization of parameters 1 to 8. **(a)** Aneurysm volume; **(b)** aneurysm centerline length; (**c**) maximum cross-sectional radius of the aneurysm; (**d**) mean cross-sectional radius of the aneurysm; **(e)** mean cross-sectional radius of the parent vessel; **(f)** ratio of the mean radius of the aneurysm to the mean radius of the parent vessel; **(g)** ratio of the mean cross-sectional diameter of the aneurysm to the centerline length; **(h)** cosine of the angle between the centerline of the parent vessel and the aneurysm centerline.

This study used the optimal *K* value obtained after discretization to cluster each parameter, and the results are shown in **Figure 3**.

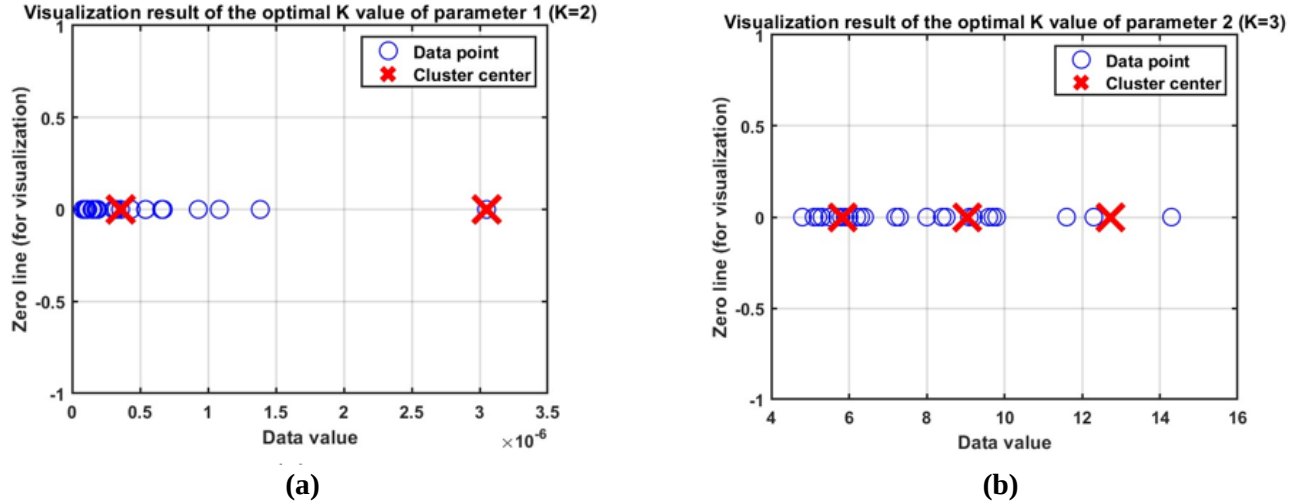

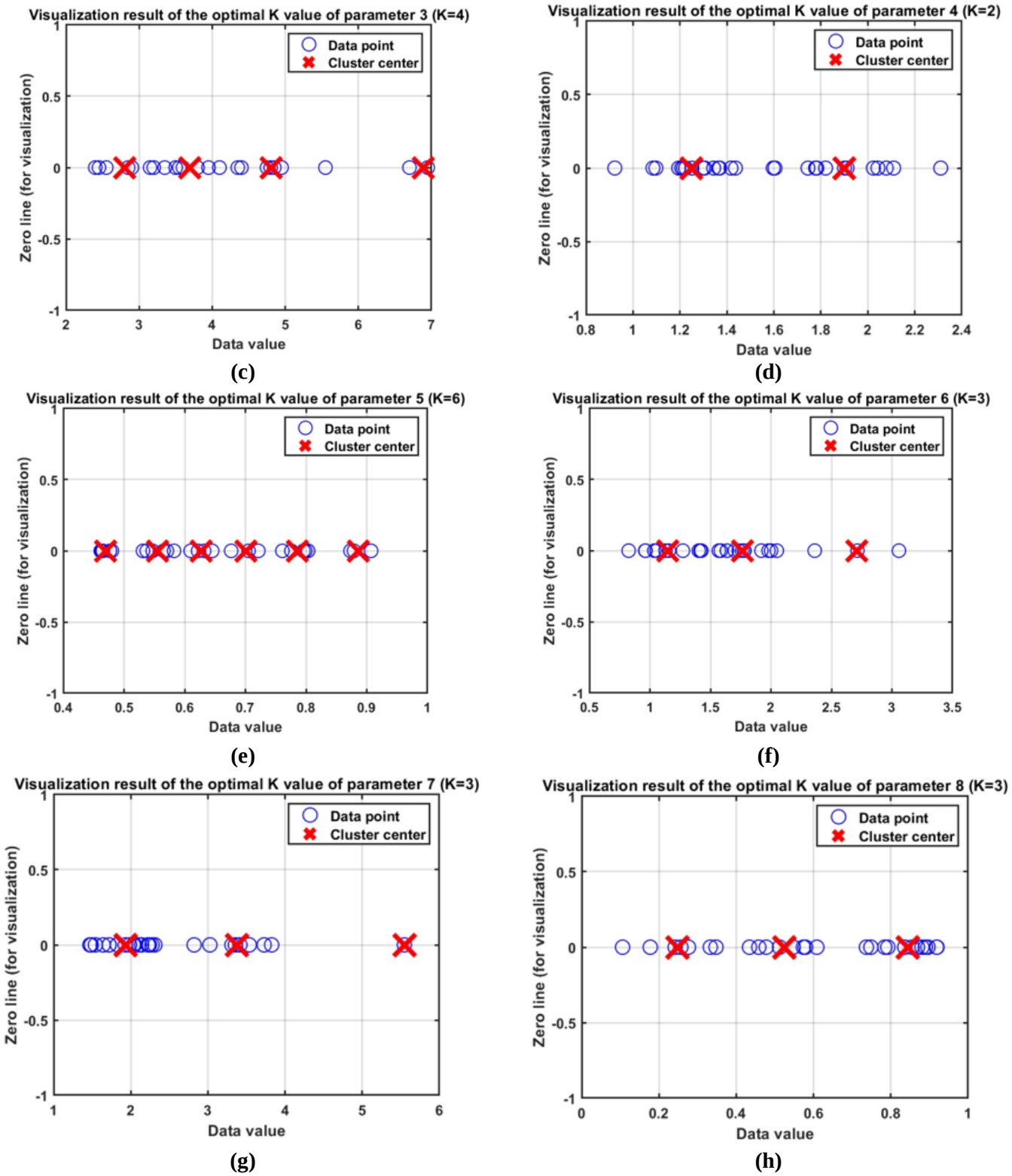

Figure 3. Clustering of parameters 1 to 8. **(a)** Aneurysm volume; **(b)** aneurysm centerline length; **(c)** maximum cross-sectional radius of the aneurysm; **(d)** mean cross-sectional radius of the aneurysm; **(e)** mean cross-sectional radius of the parent vessel; **(f)** ratio of the mean radius of the aneurysm to the mean radius of the parent vessel; **(g)** ratio of the mean cross-sectional diameter of the aneurysm to the centerline length; **(h)** cosine of the angle between the centerline of the parent vessel and the aneurysm centerline.

2.4.2. Information gain of parameters

In the process of constructing the decision tree model for the treatment of intracranial aneurysms with temperature-sensitive embolic agents, this study selects information gain as an important metric for evaluating the optimal splitting attribute. The information entropy $H(D)$ is used to measure the purity of the case set, as shown in Equation (11).

$$H(D) = -\sum_{k=1}^{n} p_k \log_2(p_k) \tag{11}$$

Where p_k represents the proportion of cases in class k among the total cases, and $\log_2(p_k)$ is the logarithm of p_k with base 2. Whenp_k equals 0, $p_k \log_2(p_k)$ is also considered to be 0. The minimum value of information entropy is 0, indicating that the case set is completely pure, meaning all cases belong to the same category.

To reflect the differences in the number of cases contained in different branch nodes, this study assigns a weight to each branch node as $\frac{|D_v|}{|D|}$, where $|D_v|$ is the number of cases in branch node v and $|D|$ is the total number of cases in the dataset. Branch nodes with a larger number of cases will have a greater influence on the overall information gain.

Based on the entropy of each branch and its weight, the overall "information gain" obtained from using attribute a to partition the sample set D can be calculated as shown in Equation (12).

$$\text{Gain}(D, a) = \text{Ent}(D) - \sum_{v=1}^{V} \frac{|D_v|}{|D|} \text{Ent}(D_v) \tag{12}$$

Where $\text{Ent}(D)$ is the overall entropy before partitioning, $\text{Ent}(D_v)$ is the entropy of branch node v. The greater the information gain, the greater the "purity improvement" achieved by using attribute a for partitioning.

This article uses the ID3 algorithm based on information gain to construct the decision tree. Information gain is a key criterion for selecting partition attributes in the decision tree. The ID3 algorithm (Quinlan, 1986) selects the attribute a^* that maximizes information gain at each step, as shown in Equation (13).

$$a^* = \arg\max_{a \in A} \text{Gain}\,(D, a) \tag{13}$$

The information gain-based selection method ensures that the decision tree effectively reduces system uncertainty at each partition, thus constructing an efficient and accurate classification decision tree. The entropy and information gain of each parameter in the model are shown in **Table 1**.

Table 1. Entropy values and information gain for each parameter.

Parameter	Entropy	Information Gain
V_{anu}(Parameter 1)	1.943	0.064
$anu_{l_{centerline}}$(Parameter 2)	1.299	0.032
anu_r^{max}(Parameter 3)	1.410	0.002

Table 1. (*Continued*).

Parameter	Entropy	Information Gain
anu_r^{mean}(Parameter 4)	1.068	0.015
$vessel_r^{mean}$(Parameter 5)	0.996	0.011
$V_ratio_{vessel}^{anu}$(Parameter 6)	1.375	0.048
$ratio_{anu_r^{mean}}^{anu_{l_{centerline}}}$(Parameter 7)	2.512	0.257
cos_{vessel}^{anu}(Parameter 8)	1.530	0.048

2.4.3. Pruning of decision tree model

Pruning is an important optimization step in the decision tree model. It simplifies the tree structure to enhance the model's generalization ability, interpretability, and computational efficiency while reducing the impact of noise. By applying appropriate pruning, the decision tree can better adapt to the data encountered in practical applications, thereby improving the overall performance of the model. In this study, pruning is utilized to optimize the decision tree by removing branches that are not strongly associated with the outcome. This process aims to streamline the tree structure, allowing the model to retain key features while eliminating redundant branches, thus enhancing the model's interpretability and computational efficiency.

2.4.4. Evaluation of the classification performance of the decision tree model

This study employs the Leave-One-Out Cross Validation (LOOCV) method to evaluate the performance of the decision tree model [35]. This approach is suitable for small sample datasets, maximizing the utilization of the training set while ensuring that each sample can independently serve as a test set. In 28 independent training and testing iterations, one sample is left out as the test set in each iteration, while the remaining 27 samples are used for model training. This cross-validation method not only enhances the robustness of the evaluation but also provides insights into the model's performance on each individual sample, allowing for a comprehensive understanding of its generalization ability. The classification performance of the decision tree model is assessed using accuracy, specificity, sensitivity, and F1-score.

3. Results

3.1. Fluid dynamics characteristics of applicable and non-applicable cases

This study determines the success of embolization treatment based on simulation results, specifically assessing whether a case is suitable for treatment. In successful embolization cases, the embolic agent is uniformly injected into the aneurysm and fully fills the aneurysmal cavity, as shown in **Figure 4**. Conversely, in unsuccessful cases, the embolic agent fails to completely fill the aneurysm and may flow into the parent artery, posing a risk of occlusion to the parent artery and its branching vessels. The simulation results for successful and unsuccessful embolization treatments are depicted in **Figure 5a,b**, respectively.

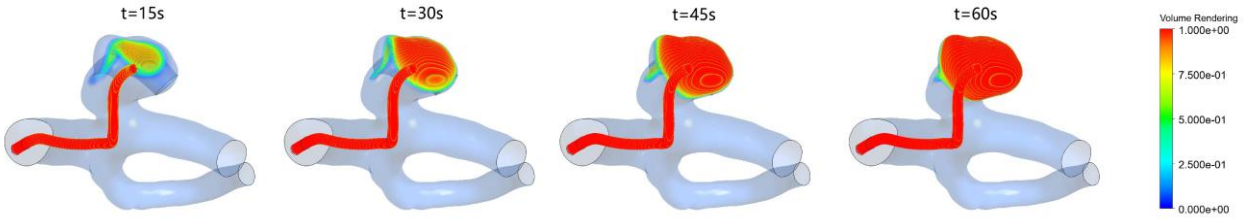

Figure 4. The diffusion process of the embolic agent in successful cases, showing the diffusion status at 15 s, 30 s, 45 s, and 60 s from left to right.

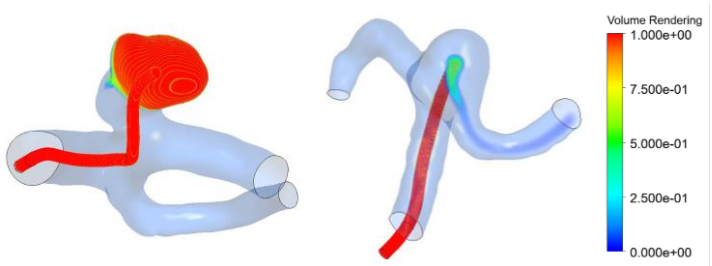

(a) **(b)**

Figure 5. Simulation results of embolization treatment. **(a)** A successful case where the embolic agent is uniformly injected into the aneurysm and completely fills the aneurysmal cavity; **(b)** a failed case where the embolic agent cannot fill the entire aneurysm, leading to flow into the parent artery and posing a risk of obstructing the parent artery and its branches.

3.2. Establishment of a binary classification decision tree model based on geometric features

The Decision Tree Constructed from Geometric Parameter Calculations is shown in **Figure 6**.

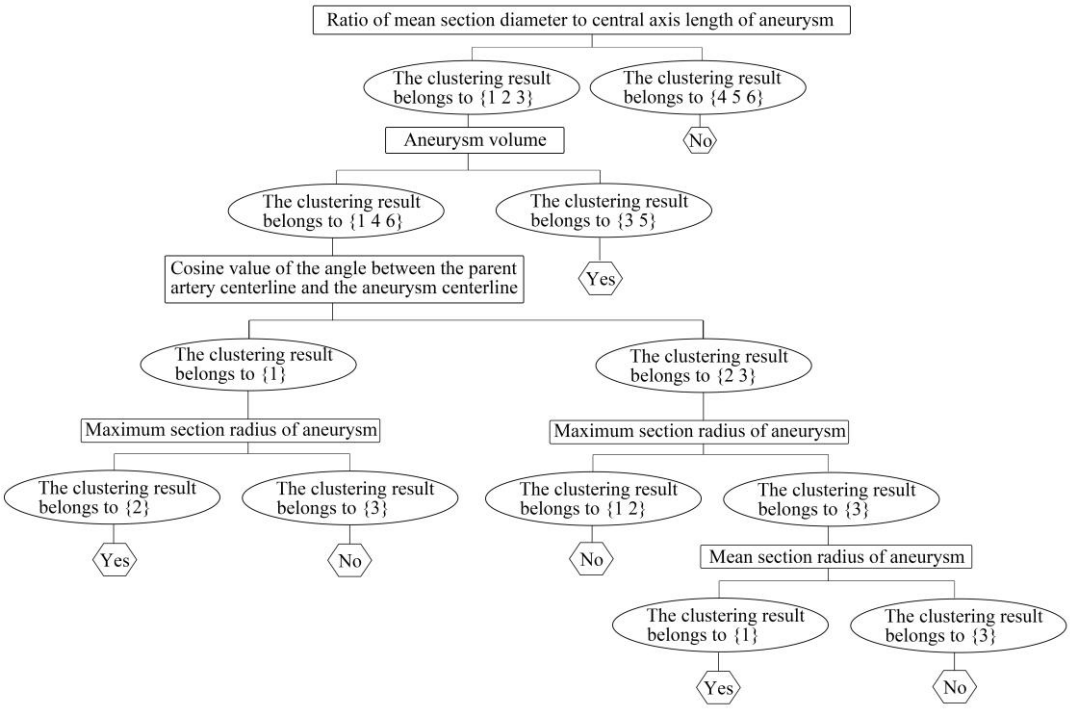

Figure 6. Decision tree model diagram.

The decision tree model underwent pruning operations to reduce the impact of noise, and the pruned decision tree is shown in **Figure 7**.

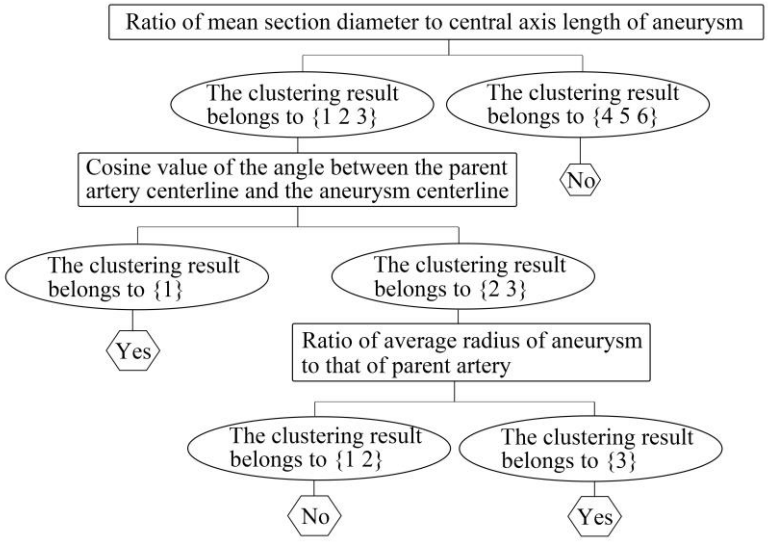

Figure 7. Pruned decision tree model.

The successful branches of the decision tree include:

1) If the ratio of the mean cross-sectional diameter of the aneurysm to the centerline length is {1, 2, 3} and the cosine of the angle between the centerline of the parent vessel and the aneurysm centerline is {1}, this branch indicates that when the ratio of the mean cross-sectional diameter to the centerline length is small and the cosine value of the angle is very small, the case is predicted to be suitable.
2) If the ratio of the mean cross-sectional diameter of the aneurysm to the centerline length is {1, 2, 3}, the cosine of the angle between the centerline of the parent vessel and the aneurysm centerline is {2, 3}, and the ratio of the mean radius of the aneurysm to the mean radius of the parent artery is {3}, this branch indicates that when the ratio of the mean cross-sectional diameter of the aneurysm to the centerline length is small, the cosine value of the angle is large, and the ratio of the mean radius of the aneurysm to the mean radius of the parent artery is very large, the case is predicted to be suitable.

The failure branches of the decision tree include:

1) If the ratio of the mean cross-sectional diameter of the aneurysm to the centerline length is {4, 5, 6}, this branch indicates that when the ratio is large, the case is predicted to be unsuitable.
2) If the ratio of the mean cross-sectional diameter of the aneurysm to the centerline length is {1, 2, 3}, the cosine of the angle between the centerline of the parent vessel and the aneurysm centerline is {2, 3}, and the ratio of the mean radius of the aneurysm to the mean radius of the parent artery is {1, 2}, this branch indicates that when the ratio is small, the cosine value is large, and the ratio of the mean radius of the aneurysm to the mean radius of the parent artery is small, the case is predicted to be unsuitable.

In constructing the final decision tree, only three key parameters are involved. Compared to the individual geometric parameters of the aneurysm and parent artery

(such as the mean cross-sectional radius, volume, centerline length, and maximum cross-sectional radius of the aneurysm, as well as the mean cross-sectional radius of the parent artery), the correlated parameters (i.e., the ratio of the mean radius of the aneurysm to the mean radius of the parent artery, the ratio of the mean cross-sectional diameter of the aneurysm to the centerline length, and the absolute value of the cosine of the angle between the centerline of the parent vessel and the aneurysm centerline) show higher information gain. This indicates that the morphology of the aneurysm and its relative position to the parent artery have a more decisive influence on the prediction results in the decision tree model.

3.3. Geometric features of suitable cases

This study analyzes the geometric features of suitable cases based on specific instances of intracranial aneurysms.

Impact of Aneurysm Morphology on Outcomes: The morphology of an aneurysm is determined by the ratio of the mean cross-sectional diameter of the aneurysm to the centerline length. By controlling two other variables to remain approximately constant, two cases with significant differences in the ratio of the mean cross-sectional diameter of the aneurysm to the centerline length were selected for analysis. In **Figure 8a**, the case with a smaller ratio resulted in treatment failure, as the embolic agent did not adequately fill the aneurysm and instead flowed into the parent artery. In contrast, **Figure 8b** illustrates a case with a larger ratio that achieved treatment success, wherein the embolic agent effectively filled the aneurysm, as shown in **Figure 8**.

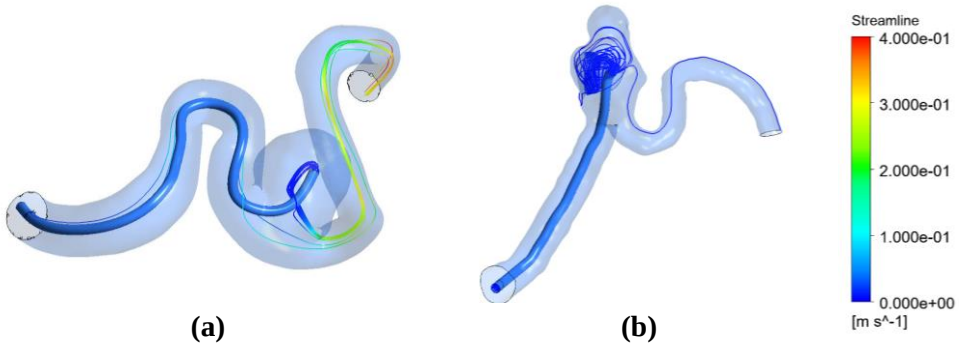

Figure 8. Comparison of the ratio of the mean cross-sectional diameter of the aneurysms to the centerline length. **(a)** Case with small ratios; **(b)** case with high rates

Impact of Relative Size of Aneurysm and Parent Artery on Outcomes: The ratio of the mean radius of the aneurysm to the mean radius of the parent artery is a key parameter for assessing their relative sizes. By keeping the other two parameters approximately constant, two cases with different ratios of the mean radius of the aneurysm to the mean radius of the parent artery were selected for analysis. This illustrates the importance of larger aneurysms in treatment strategy selection. In **Figure 9a**, where the aneurysm is smaller relative to the parent artery, the blood flow velocity is higher, making it difficult for the embolic agent to adequately fill the aneurysm. Conversely, when the aneurysm is larger relative to the parent artery, as

shown in **Figure 9b**, the blood flow velocity within the aneurysm is relatively slower, as illustrated in **Figure 9**.

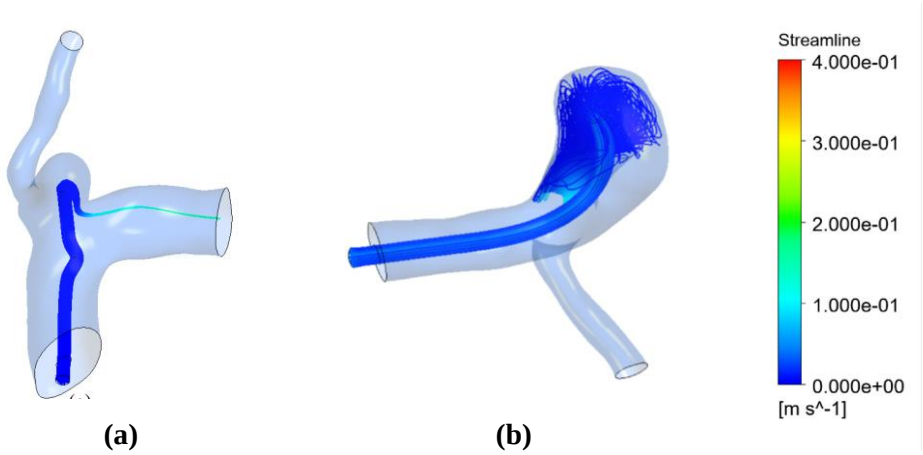

(a) **(b)**

Figure 9. Comparison of the ratio of the mean radius of the aneurysm to the mean radius of the parent artery. **(a)** Case with small ratios; **(b)** case with high rates.

The Impact of the Angle between the Centerline of the Parent Artery and the Centerline of the Aneurysm on Decision-Making: The absolute value of the cosine of the angle between the centerline of the parent artery and the centerline of the aneurysm is an important geometric parameter used to quantify their relative orientation. By keeping the other two parameters approximately constant, two cases with different angles between the centerlines were selected to explore the specific impact of this geometric parameter on clinical decision-making. In **Figure 10a**, the presence of a significant jet flow makes it difficult for the embolic agent to adequately fill the aneurysm, resulting in treatment failure. Conversely, when the centerline of the parent artery is nearly perpendicular to the centerline of the aneurysm, as shown in **Figure 10b**, the flow within the aneurysm predominantly exhibits a shear flow pattern without significant jet impact. This blood flow characteristic increases the likelihood of successful embolization, as the shear flow can more effectively restrict non-target movement of the embolic agent, thereby enhancing the local treatment effect, as illustrated in **Figure 10**.

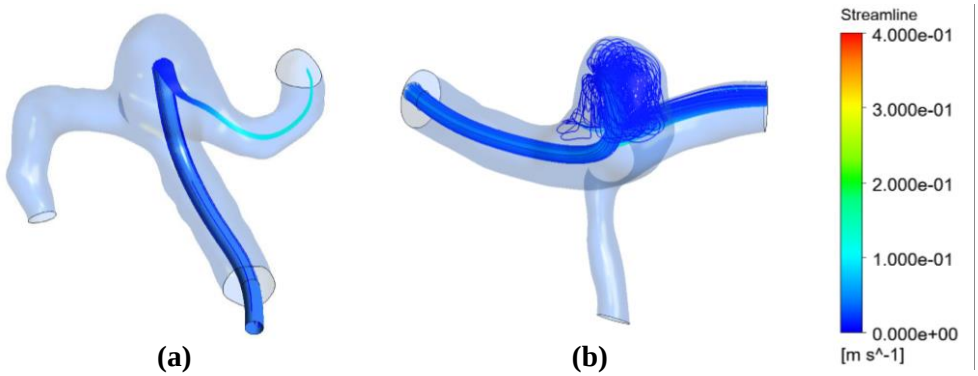

(a) **(b)**

Figure 10. Comparison of the angle between the centerline of the parent artery and the centerline of the aneurysm. **(a)** Case with large clip angles; **(b)** Case where the angle tends to be perpendicular

3.4. Evaluations of the classification performance of the decision tree model

After cross-validation, the success rate for positive cases was 71.43%, while the success rate for negative cases was 80.95%, resulting in an overall success rate of 78.57%. This indicates that the model demonstrates favorable predictive performance across all samples. The model's sensitivity is 71.4%, effectively identifying the majority of positive cases, while its specificity is 81.0%, reflecting a relatively low misclassification rate among negative cases. Additionally, the model's F1 score is 62.5%, achieving a balance between precision and recall for positive samples.

4. Discussion

This study utilized the Euler two-phase flow model to simulate blood flow within the aneurysm and its coupling behavior with temperature-sensitive embolic agents, resulting in virtual treatment outcomes for intracranial aneurysms. By further incorporating the geometric structures of the aneurysm and the parent artery, a decision tree model was developed based on these geometric features for the treatment of intracranial vascular malformations using temperature-sensitive embolic agents. According to the final model results, the primary factors influencing the success of embolization treatment were found to be the relative position and size of the aneurysm and parent artery, specifically the ratio of the mean cross-sectional diameter of the aneurysm to the centerline length, the ratio of the mean radius of the aneurysm to the mean radius of the parent artery, and the absolute value of the cosine of the angle between the centerlines of the parent artery and the aneurysm.

For the ratio of the mean cross-sectional diameter of the aneurysm to the centerline length, a smaller ratio indicates a more elongated shape of the aneurysm, providing ample space for the development of the jet flow within. In such cases, the energy dissipation caused by shear effects is relatively large, effectively reducing the direct impact of the jet. Consequently, the kinetic energy of the jet is diminished, which helps decrease the risk of the embolic agent being displaced by the jet flow, thereby increasing the success rate of embolization. This physical phenomenon suggests that elongated aneurysms may have a higher therapeutic adaptability and success probability during treatment.

Regarding the ratio of the mean radius of the aneurysm to the mean radius of the parent artery, a larger ratio indicates a greater size of the aneurysm relative to the parent artery. Analysis from the decision tree model shows a tendency to select relatively larger aneurysms, which are clinically categorized as giant aneurysms. This characteristic helps reduce the risk of the embolic agent quickly flowing into the parent artery due to hemodynamic impacts, thus enhancing the success rate of treatment.

As for the absolute value of the cosine of the angle between the centerline of the parent artery and the centerline of the aneurysm, values close to 0 indicate that the two are nearly perpendicular; conversely, values near 1 suggest that they are parallel, a configuration commonly seen in dome-shaped aneurysms. According to the decision tree model presented in this study, selecting aneurysms with a vertical configuration shows a strong correlation with predicting treatment success, likely due to more favorable hemodynamic conditions for intervention in such configurations.

In this paper, a decision tree prediction model based on geometric features is constructed, and a method is proposed to rapidly predict the treatment effect without relying on complex computational fluid dynamics (CFD) simulations. Compared with the disadvantages of CFD simulation, which is difficult to be widely applied in clinical practice due to its time-consuming and high computational cost, the model in this paper is able to quickly and efficiently determine whether an aneurysm is suitable for treatment with a temperature-sensitive embolic agent by analyzing the geometric features of the intracranial aneurysm, which greatly simplifies the computational process, and improves the operability and applicability in clinical practice. In clinical practice, the prediction model proposed in this paper provides physicians with an auxiliary screening tool to quickly determine whether a case is suitable for temperature-sensitive embolic agent treatment through geometric features before surgery, thereby reducing surgical risks and improving the efficiency and accuracy of personalized treatment. This technical tool lays the foundation for physicians to formulate more accurate treatment plans, which helps to increase the success rate of surgery and improve the prognosis of patients, and promotes the further development of intracranial aneurysm treatment based on temperature-sensitive embolic agents.

However, this study has several limitations. Each aneurysm was modeled as extending from a relative center position, and only three intervention locations were considered to manage computational costs; in reality, the positioning of microcatheters during treatment may be more complex than accounted for in this study. The coagulation process of the embolic agent is not instantaneous; early coagulation may obstruct blood flow. Future research could enhance the model's realism by improving constitutive relationships and incorporating time-dependent factors. Although a decision tree model with good classification performance was achieved with a relatively small sample size, increasing the sample size will be an important aspect for future studies to consider. Integration of models into healthcare information systems requires additional hardware and software support, especially in geometric feature extraction. If model predictions conflict with physician judgment, physician experience should be prioritized and models should be adjusted through multidisciplinary discussions. Future research could focus on optimizing the model to provide feedback on decision-making conflict cases through treatment outcomes.

5. Conclusion

This study implemented computational simulations of temperature-sensitive embolic agents for the treatment of intracranial aneurysms using the Euler two-phase flow model. Based on the CFD simulation results, a decision tree model was constructed that incorporates geometric features. The findings indicate that the relative position and size of the parent artery and aneurysm significantly affect the outcomes of embolization treatment. Aneurysm cases that are suitable for treatment with temperature-sensitive embolic agents typically exhibit the following characteristics: a smaller ratio of the mean cross-sectional diameter of the aneurysm to the centerline length, a larger ratio of the mean radius of the aneurysm to the mean radius of the parent artery, and a near-vertical orientation between the centerline of the parent artery and that of the aneurysm. The proposed decision tree prediction model based on

geometric features requires only the integration of clinical imaging data to identify suitable cases, thus saving time and computational costs while serving as an auxiliary tool to enhance the success rate of surgical interventions.

Author contributions: Conceptualization, ML and YW; methodology, BY; software, ML; validation, ML, BY and YW; formal analysis, BY; investigation, ML; resources, ML; data curation, BY; writing—original draft preparation, BY; writing—review and editing, BY; visualization, YW; supervision, ML; project administration, ML; funding acquisition, ML. All authors have read and agreed to the published version of the manuscript.

Ethical approval: Not applicable.

Conflict of interest: The authors declare no conflict of interest.

References

1. Byoun H S, Huh W, Oh C W, et al. Natural history of unruptured intracranial aneurysms: a retrospective single center analysis [J]. J Korean Neurosurg Soc, 2016, 59(1): 11-16.
2. Zhao J, Lin H, Summers R, et al. Current treatment strategies for intracranial aneurysms: an overview [J]. Angiology, 2018, 69(1): 17-30.
3. Kim S, Nowicki K W, Gross B A, et al. Injectable hydrogels for vascular embolization and cell delivery: The potential for advances in cerebral aneurysm treatment [J]. Biomaterials, 2021, 277: 121109, doi: 10.1016/j.biomaterials.2021.121109.
4. Kang X-K, Guo S-F, Lei Y, et al. Endovascular coiling versus surgical clipping for the treatment of unruptured cerebral aneurysms: Direct comparison of procedure-related complications [J]. Medicine, 2020, 99(13): e19654, doi: 10.1097/MD.0000000000019654.
5. Chai C L, Pyeong Jeon J, Tsai Y-H, et al. Endovascular intervention versus surgery in ruptured intracranial aneurysms in equipoise: a systematic review [J]. Stroke, 2020, 51(6): 1703-1711.
6. Han Y M, Lee J Y, Choi I J, et al. Endoscopic removal of a migrated coil after embolization of a splenic pseudoaneurysm: a case report[J]. Clinical Endoscopy, 2014, 47(2): 183-187.
7. Kashkoush A, El-Abtah M E, Petitt J C, et al. Flow diversion for the treatment of intracranial bifurcation aneurysms: a systematic review and meta-analysis[J]. Journal of NeuroInterventional Surgery, 2024, 16(9): 921-927.
8. Zou R, Guo K, Wang T, et al. E-239 Intra-saccular flow disruptors for intracranial aneurysms treatment: mechanisms of occlusion and predictive parameters[J]. 2024.
9. Pineda-Castillo S A, Stiles A M, Bohnstedt B N, et al. Shape memory polymer-based endovascular devices: design criteria and future perspective [J]. Polymers, 2022, 14(13): 2526.
10. Tevah J, Senf R, Cruz J, et al. Endovascular treatment of complex cerebral aneurysms with onyx hd-500® in 38 patients [J]. J Neuroradiol, 2011, 38(5): 283-290.
11. Rodriguez J N, Hwang W, Horn J, et al. Design and biocompatibility of endovascular aneurysm filling devices[J]. J Biomed Mater Res A. 2015, 103(4): 1577-1594.
12. Ko G, Choi J W, Lee N, et al. Recent progress in liquid embolic agents [J]. Biomaterials, 2022, 287: 121634.
13. Fan R-R, Liu Y-B, Zhang T, et al. Based on clinical application research progress of thermosensitive gel in different drug delivery sites [J]. Acta Pharm Sin B, 2022, 1235-1244.
14. Li X, Ullah M W, Li B, et al. Recent Progress in Advanced Hydrogel‐Based Embolic Agents: From Rational Design Strategies to Improved Endovascular Embolization [J]. Adv Healthc Mater, 2023, 12(17): 2202787.
15. Murayama Y, Viñuela F, Tateshima S, et al. Endovascular treatment of experimental aneurysms by use of a combination of liquid embolic agents and protective devices [J]. AJNR Am J Neuroradiol, 2000, 21(9): 1726-1735.
16. Umeda Y, Ishida F, Tsuji M, et al. Computational fluid dynamics (CFD) using porous media modeling predicts recurrence after coiling of cerebral aneurysms [J]. PLoS One, 2017, 12(12): e0190222, doi: 10.1371/journal.pone.0190222.
17. Damiano R J, Ma D, Xiang J, et al. Finite element modeling of endovascular coiling and flow diversion enables hemodynamic prediction of complex treatment strategies for intracranial aneurysm [J]. J Biomech, 2015, 48(12): 3332-3340.

18. Wang Y, Leng X, Zhou X, et al. Hemodynamics in a middle cerebral artery aneurysm before its growth and fatal rupture: case study and review of the literature [J]. World Neurosurg, 2018, 119: e395-e402, doi: 10.1016/j.wneu.2018.07.174.
19. Leng X, Wang Y, Xu J, et al. Numerical simulation of patient-specific endovascular stenting and coiling for intracranial aneurysm surgical planning [J]. J Transl Med, 2018, 16: 1-10.
20. Brinjikji W, Kallmes D F, Kadirvel R J. Mechanisms of healing in coiled intracranial aneurysms: a review of the literature [J]. AJNR Am J Neuroradiol, 2015, 36(7): 1216-1222.
21. Liu Y, Zhang S, Bai S, et al. Hemodynamic and morphological analysis of mirrored internal carotid-posterior communicating artery aneurysms and their impact on aneurysm rupture [J]. Chinese Journal of Cerebrovascular Diseases, 2022, 19(11): 741-748.
22. Gasser T C, Nchimi A, Swedenborg J, et al. A novel strategy to translate the biomechanical rupture risk of abdominal aortic aneurysms to their equivalent diameter risk: method and retrospective validation [J]. Eur J Vasc Endovasc Surg, 2014, 47(3): 288-295.
23. Cebral J R, Mut F, Weir J, et al. Quantitative characterization of the hemodynamic environment in ruptured and unruptured brain aneurysms [J]. AJNR Am J Neuroradiol, 2011, 32(1): 145-151.
24. Schena M, Testa F, Bozzetto M, et al. A CFD-based framework to evaluate surgical alternatives in cerebral aneurysms[J]. Computer Methods in Biomechanics and Biomedical Engineering: Imaging & Visualization, 2024, 12(1): 2325351.
25. Babiker M H, Chong B, Gonzalez L F, et al. Finite element modeling of embolic coil deployment: multifactor characterization of treatment effects on cerebral aneurysm hemodynamics[J]. Journal of Biomechanics, 2013, 46(16): 2809-2816.
26. Ostrowski Z, Melka B, Adamczyk W, et al. CFD analysis of multiphase blood flow within aorta and its thoracic branches of patient with coarctation of aorta using multiphase Euler-Euler approach [J] Phys Conf Ser, 2016, 745: 032112, doi: 10.1088/1742-6596/745/3/032112.
27. Orlowski P, Al-Senani F, Summers P, et al. Towards treatment planning for the embolization of arteriovenous malformations of the brain: intranidal hemodynamics modeling[J]. IEEE transactions on biomedical engineering, 2011, 58(7): 1994-2001.
28. Zhang B, Chen X, Zhang X, et al. Computational modeling and simulation for endovascular embolization of cerebral arteriovenous malformations with liquid embolic agents [J]. Acta Mech Sin, 2024, 40(1): 623042.
29. Perktold K, Peter R O, Resch M, et al. Pulsatile non-Newtonian blood flow in three-dimensional carotid bifurcation models: a numerical study of flow phenomena under different bifurcation angles[J]. Journal of biomedical engineering, 1991, 13(6): 507-515.
30. Hodis S, Kargar S, Kallmes D F, et al. Artery length sensitivity in patient-specific cerebral aneurysm simulations[J]. American Journal of Neuroradiology, 2015, 36(4): 737-743.
31. Pereira V M, Brina O, Gonzales A M, et al. Evaluation of the influence of inlet boundary conditions on computational fluid dynamics for intracranial aneurysms: a virtual experiment[J]. Journal of biomechanics, 2013, 46(9): 1531-1539.
32. Song Y-Y, Ying L J. Decision tree methods: applications for classification and prediction [J]. Shanghai Arch Psychiatry, 2015, 27(2): 130.
33. Ivantsits M, Huellebrand M, Kelle S, et al. Intracranial aneurysm rupture risk estimation utilizing vessel-graphs and machine learning[C] //Cerebral Aneurysm Detection and Analysis: First Challenge, Lima: CADA 2020, 2020: 93-103.
34. ANSYS Official Website. Software Overview [EB/OL]. https://www.ansys.com, 2024-08-01/2024-08-15.
35. Wong, Tzu-Tsung. Performance evaluation of classification algorithms by k-fold and leave-one-out cross validation[J]. Pattern recognition, 2015, 48(9): 2839-2846.